

Interferometric techniques for fundamental static or dynamic pressure measurements and transducer calibration

To cite this article: R Jones and B D Bergquist 1977 *J. Phys. E: Sci. Instrum.* **10** 1265

View the [article online](#) for updates and enhancements.

You may also like

- [Improvement of the photopolymerization and bottom-curing performance of benzocarbazole oxime ester photoinitiators with red-shifted absorption](#)
Kaori Sameshima, Hisatoshi Kura, Yuki Matsuoka et al.
- [Safety of arterial shear wave elastography—ex-vivo assessment of induced strain and strain rates](#)
Tim Nordenfur, Kenneth Caidahl, Dmitry Grishenkov et al.
- [Effects of pressure variation and atrial fibrillation on CardioMEMS™ HF measured pulmonary artery diastolic pressure: comparison of device-averaged and visually inspected waveforms](#)
Aaron M Wolfson, Omid Yousefian, Lindsay Short et al.

Interferometric techniques for fundamental static or dynamic pressure measurements and transducer calibration

R Jones and B D Bergquist

Department of Mechanical Engineering, Loughborough University of Technology, Loughborough, Leics LE11 3TU, UK

Received 7 April 1977, in final form 24 August 1977

Abstract New techniques for the interferometric measurement of quasi-static and dynamic pressure variations are discussed. The pressure variations are transmitted through oil contained in a closed cavity and the measurements depend on an experimental calibration constant derived solely from measurements of mass and length. The sensitivities of the interferometers (a Michelson and a Jamin) are adjusted so that pressure variations produce phase changes of less than $\pm \pi/2$; this then allows the pressure variations to be directly displayed. In an application of the technique pressure transducers are calibrated by mounting the elements in the side of the cavity. Their outputs are then compared with pressure variations measured over the frequency range from 0 (quasi-static pressure changes) to 6 kHz.

1 Introduction

The refractive index of a fluid varies linearly with its density when the changes in density are sufficiently small (Rosen 1947, 1949). Small changes in refractive index may be accurately measured using two-beam interferometry (e.g. Born and Wolf 1969). These principles have recently been combined to form the basis of interferometric manometers for static and dynamic measurement (Butters and Bergquist 1969, Thomson and Tanner 1969). In both these systems the fluid was a low-viscosity oil having a compressibility of the order of 10^6 kPa, and pressure variations of typical maximum magnitude 10^8 kPa were applied. Under these conditions the linear relationship between refractive index and density is satisfied and fluctuations in temperature are negligible so that the refractive index measurement is directly related to the applied pressure. The work described in this paper is based on the same principles; however, two significant limitations are inherent in the original devices:

- (i) The fringe shifts were photographically recorded, and a single pressure measurement was a lengthy process of photographic recording and point-by-point fringe trace analysis.
- (ii) The observation of erroneous fringe shifts, resulting from movements being transmitted from the source of pressure excitation into the optical components, was not considered.

These limitations have now been eliminated in that the pressure changes are directly displayed. This is achieved by adjusting the sensitivity of the interferometer so that the applied pressure produces a phase shift of less than $\pm \pi/2$. One is also able to detect regions of measurement where errors due to (ii) arise. New solutions to the problems of obtaining a perfectly air-free oil cavity and optimising the efficiency of the coupling between the source of pressure excitation and the oil cavity are also discussed.

In an application of the technique transducers are calibrated by mounting the transducer in the cavity wall and comparing their output with the interferometrically measured pressure. This observation is now extended by using electronic speckle pattern and holographic interferometry to observe simultaneously the deflection of the element (Jones and Bergquist 1976). The precise interpretation of the results requires that the mean pressure change throughout the cavity, as detected by the interferometer (see §2.2), be related to the pressure at the region in the cavity where the transducer is mounted. A theoretical analysis is presented which gives the necessary correction factor over the frequency range 0–10 kHz. This general characteristic of interferometric pressure measurement does not appear to have been discussed in previous publications.

2 Theory

2.1 The pressure distribution within the oil cavity for quasi-static and dynamic excitation

Let us consider figure 1. Air-free oil is contained in a cylindrical cavity of length l and of unit cross-sectional area. An airtight piston of circular cross section and radius r is mounted

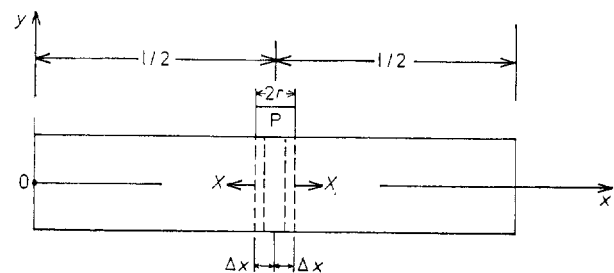


Figure 1 The geometry of the oil cavity.

with its central axis parallel to the y axis so that it intersects the central x axis of the cavity at $x = l/2$. In its equilibrium position the face of the piston is flush with the upper surface of the cavity bore. For dynamic measurements the piston P is coupled to an external electromagnetic vibrator which is sinusoidally driven; this causes the piston to perform forced simple harmonic motion about its position of equilibrium. The pressure distribution in the cavity that results from this form of excitation is now calculated. It is clear (a) that the fluid motion will be asymmetric about $x = l/2$ and (b) that apart from a small central region ($x = l/2 \pm \Delta x$) the displacement will be uniform across the bore of the cell (i.e. equivalent to that produced by two pistons lying in the y - z plane and moving in equal and opposite directions along the x axis; these are shown by the broken lines in figure 1). The boundary conditions at $x = l/2 \pm \Delta x$ can therefore be written as

$$\Delta p(l/2 \pm \Delta x) = -K_a \left(\frac{\partial X}{\partial x} \right)_{x=l/2 \pm \Delta x} \quad (1)$$

where Δp is the pressure increment, K_a the adiabatic compressibility of the fluid and X the fluid displacement parallel to

Interferometric pressure measurement

inclination of the end faces of the cavity – see figures 3 and 4); and $\partial n/\partial p$ is the variation of refractive index n with respect to pressure p .

By the Gladstone–Dale relationship (Rosen 1947, 1949) $\partial n/\partial p = (n_0 - 1)/\rho_0$ where n_0 and ρ_0 are, respectively, the equilibrium refractive index and density. Furthermore $\partial p/\partial \rho = K_a/\rho_0$; therefore

$$\frac{\partial n}{\partial p} = \frac{n_0 - 1}{K_a} \quad (12)$$

Combining equations (11) and (12) gives the result

$$\Delta\phi_{12} = \Lambda \Delta\bar{p} \quad (13)$$

where

$$\Lambda = 2\pi/\lambda[(n_0 - 1)/K_a]L_{12}.$$

Λ is measured experimentally and calibrates the phase shift to the mean pressure variation (§4.1). (A theoretical value would be unacceptable because it would require the assumption of (i) a value for K_a and (ii) the linearity of the Gladstone–Dale relationship.) Now, the intensity in the interference pattern varies sinusoidally with respect to $\Delta\phi_{12}$ and the fringe shift detector is positioned midway between intensity minima and maxima. It therefore follows that

$$\sin \Delta\phi_{12} = \frac{\Delta V_p}{2\Delta V_c} \quad (14)$$

where ΔV_c is the voltage output due to the fringe intensity varying between maximum and minimum, and $\pm \Delta V_p/2$ is the pressure-induced voltage swing about the initial output.

It is now possible to combine the above equations with previous results (equations (9), (12)) to give the following basic equation for interferometric pressure measurement:

$$\Delta p = 2 \frac{C(\nu)}{\Lambda} \sin^{-1} \left(\frac{\Delta V_p}{\Delta V_c} \right) \quad (15)$$

where Δp is the amplitude of the pressure applied at a frequency ν Hz to the transducer mounted with its central axis intersecting the x axis at coordinate $l/4$.

Equation (15) will not be directly applicable when $|\Delta\phi_{12}/2| > \pi/2$. However, the interferometer may be operated at both high and low pressure sensitivities (Λ (Michelson)/ Λ (Jamin) = $L/s\gamma \approx 100$) and this condition can therefore generally be satisfied. A second point of breakdown will occur at frequencies where the natural wavelength of the vibration in the cavity becomes shorter than its overall length. When this occurs additional nodes at points intermediate between the piston and the cell ends will be introduced (e.g. the second resonant mode of an organ pipe of length $l/2$ would be a particular solution). Under these conditions the analysis in §2.1 would require modification. For the cavity used the theoretical value for this frequency is $\nu = (K_a/\rho)^{1/2}/l \approx 14$ kHz. A final important feature of the interferometric measurement is apparent from figures 3 and 4, where it can be seen that a second pair of fringe fields F_2 is formed by an interferometer having optical components practically common to those forming the pressure-measuring interferometer, but insensitive to the pressure changes. Fringe shifts in the F_2 field therefore indicate that an error due to interferometer motion is present in the pressure signal. It would be possible to determine a corrected value for the pressure signal if the relative phase of the error and pressure component were known. This approach was not pursued in the current work (vibration insulation is considered a more practical solution – see conclusion) and pressure measurements were only made at frequencies where the error signal was negligible with respect to the pressure signals.

2.3 The holographic and electronic speckle pattern interferometric measurements

The principles of both these techniques have been discussed in detail elsewhere (e.g. Jones and Bergquist 1976, pp 155–9) and need only be briefly summarised. In the arrangement used (see §3.2) the transducer is illuminated normally by a plane wavefront and also viewed along the transducer surface normal. A double-exposure hologram of the surface in the deformed and undeformed position may be recorded. Alternatively one may record a hologram with a continuous sinusoidal excitation applied to the transducer. In the first case fringe-defining contours of constant out-of-plane displacement d are observed and are described by the equation

$$d = N\lambda/2 \quad (16a)$$

where N is the fringe order number (assumed zero at the diaphragm boundary). For the second case fringes of a characteristic $J_0^2(4\pi d/\lambda)$ distribution are observed (Powell and Stetson 1965) and the out-of-plane vibration amplitude is given approximately by the equation

$$d = N\lambda/4 \quad (16b)$$

where $N=0$ at the vibration mode.

Identical results to those above are observed when electronic speckle pattern interferometry is used but in this case there is the advantage of non-photographic, real-time observation. The experimental details of both these techniques are discussed in the next section.

3 The apparatus and experimental technique

3.1 The oil cavity

A critical factor in the application of the technique is that consistent results can only be obtained if the oil within the cavity is bled so as to be totally air-free. Considerable attention was devoted to this problem and the final design shown in cross-sectional side elevation (figure 5) permits the cavity to be

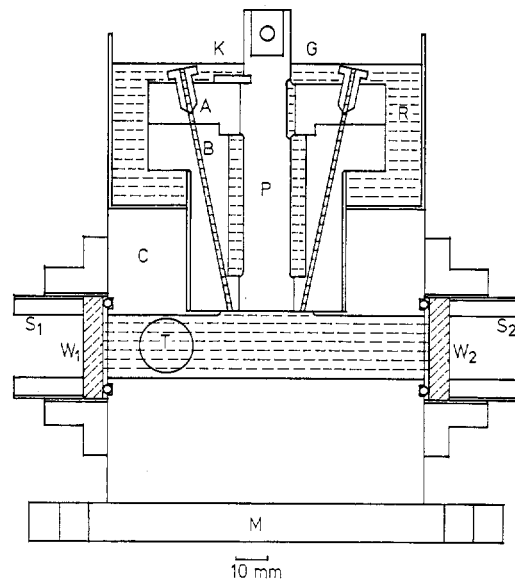


Figure 5 A cross-sectional side elevation of the oil cavity.

automatically bled *in situ* and also eliminates the entry of air during piston motion. In this figure W_1 and W_2 are optically flat cavity windows held in position against O-rings by the retaining rings S_1 and S_2 ; the transducer mounting is at T. The piston P is guided by the combination A, B which screws

into the main body of the cavity C. This total arrangement is completely immersed in oil contained in the upper reservoir R and the cavity is easily bled by opening the bleed nipples and tilting it slightly about the piston axis†. This allows any air present to rise through the bleed pipes. The gland G permits the oil to flow into the volume directly above the piston P, making the entrance of air during operation impossible. The key K holds the piston in position when the cavity is not in use and the base M bolts into the main bed of the interferometer

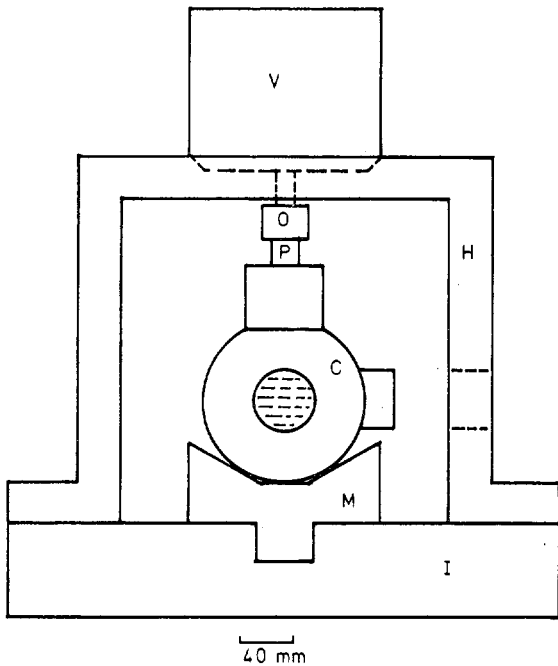


Figure 6 The coupling arrangement between the vibrator and the oil cavity.

† It is interesting to note that the design could be further improved by making the bore of the cavity taper slightly outwards from the bleed holes. The air would then rise through the bleed pipes without the cavity having to be tilted.

(I, figure 6). The piston was constructed to have airtight operation and the alignment between the source of excitation and the piston head was therefore extremely critical. When rigid coupling was used stricture and piston wear due to misalignment were found to be serious problems. These were eliminated by using the arrangement shown in figure 6. The vibrator V is mounted on a rigid, stress-relieved girder section H which is in turn bolted to the interferometer base I. The piston top has had a soft-iron core inserted and a 25 mm diameter pot magnet O has been bolted to the vibrator drive in order to form a self-aligning contact between the drive and the piston.

3.2 The interferometer

From figure 7 it may be seen how the basic pressure-measuring interferometer (in this case the Michelson arrangement) has been combined into the overall practical system. In practice the beams in the two interferometers are slightly misaligned with respect to one another and also the source laser beam. Troublesome return beams are then sufficiently displaced by the optical lever effect to be apertured out. The outputs from the light-sensitive detectors (Centronic OS15 hybrid photodiode amplifier combinations with linear response from DC to 20 kHz) are directly monitored by a storage oscilloscope, and ΔV_c and ΔV_p (equation (14)) are measured by a digital voltmeter. In the measurement of ΔV_c the fringe pattern is automatically scanned across the detector by rotating the optical flat P_4 as shown. This changes the path length of the beam in one leg of the interferometer. The remainder of the optics consists of the speckle and holographic interferometers. The unexpanded laser beam is initially split at the 95% transmitting wedge beam splitter and the stronger beam passes on to be expanded by a $\times 40$ objective L_3 and collimated by the lens L_4 . The transducer diaphragm is normally illuminated by this plane wavefront which is reflected from the 50/50 beam-splitting wedge B. An image of the diaphragm as viewed normally by lens L_6 is formed in the plane of the television camera Vidicon. The first of the two weaker beams is expanded by a $\times 20$ objective L_7 and a pinhole in combination. This speckle pattern interferometer reference beam is reflected on to the Vidicon plane via the low-loss, beam-splitting cube B_R . When a dynamic pressure variation is applied a fringe pattern corresponding to the time-averaged deflection of the diaphragm

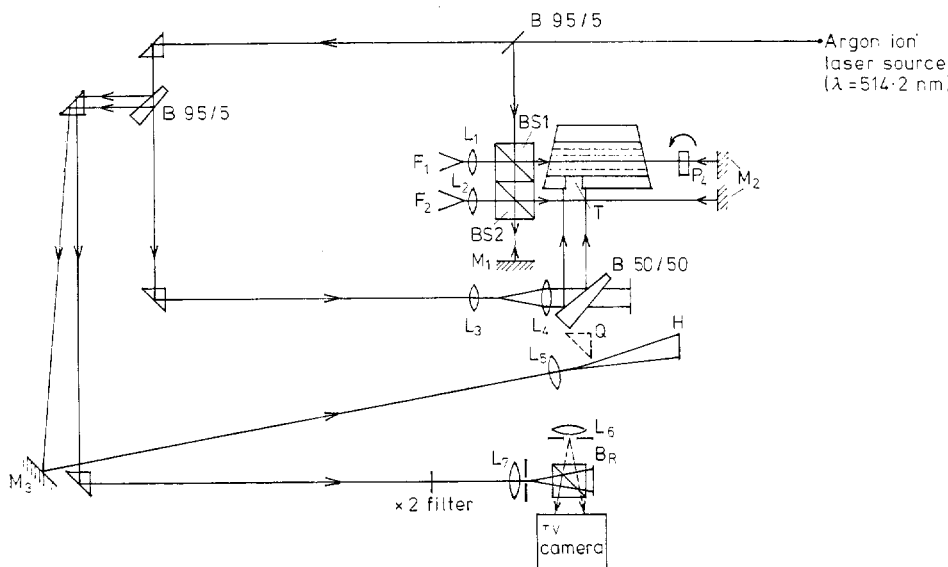


Figure 7 The overall layout of the interferometer.

Interferometric pressure measurement

(equation (16b)) is directly observed on a television monitor. (The light-integrating action of the Vidicon causes this time-averaging effect and may be regarded as being equivalent to the exposure time in time-averaged holographic interferometry.) In a second application a quasi-static pressure variation may be applied and in this case a video recording of the original state speckle pattern is electronically subtracted from the deformed state pattern observed in real time. A fringe pattern representing contours of constant out-of-plane displacement (equation (16a)) is then displayed on the monitor. Fringe resolution greater than that attainable in speckle pattern interferometry may be obtained if holographic interferograms of the deflections are recorded. It can be seen from figure 7 that the second of the two weak beams forms the reference beam for a hologram in the plane H. When a right-angled prism Q (broken outline) is placed in position, T may be observed normally from behind H. A time-averaged or static deflection interferogram can then be obtained in the usual way without disturbing the speckle pattern interferometer.

4 A summary of experimental results

4.1 Quasi-static pressure measurements

For the application of quasi-static pressure variations a circular table is attached to the top of the piston. Known masses are added to this table and gently removed when equilibrium has been reached. The resultant pressure change is regarded as quasi-static and its magnitude is determined by dividing the applied weight by the area of the piston face. Λ is measured experimentally by plotting the resultant phase shift $\Delta\phi_{12}$ against this known quasi-static pressure change Δp (figure 8).

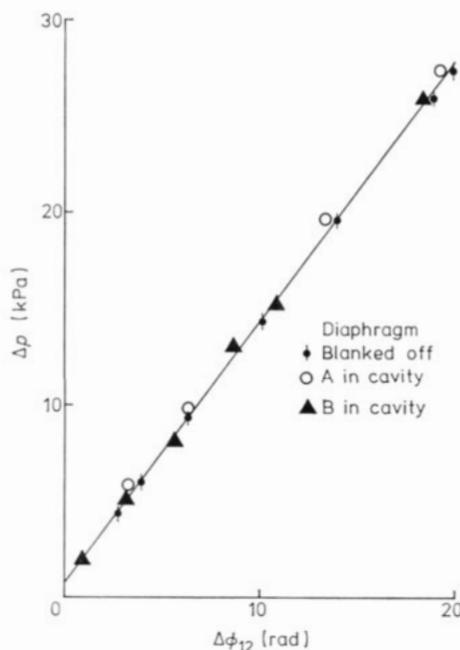


Figure 8 Sensitivity calibration graph for the Michelson interferometer. Applied quasi-static pressure Δp (kPa) is plotted against fringe shift $\Delta\phi_{12}$ (rad).

The experimental value for Λ (Michelson) measured from the gradient of this graph is 1.36 ± 0.03 kPa rad^{-1} and the value for Λ (Jamin) measured in the same way is $(4.5 \pm 0.2) \times 10^2$ kPa rad^{-1} . The uncertainties in these results are statistical in origin and are derived from the deviations from the best straight-line fit to the calibration results. The source of statistical error is in the measurement of $\Delta\phi_{12}$. In addition a systematic error arises

from the force necessary to overcome friction in the piston; this appears as the intercept on the pressure axis in figure 8. Errors in the measurement of mass and piston area are negligible and it can be also seen from figure 8 that Λ is not sensitive to the presence of different transducers. Quasi-static pressure measurements are also used in the determination of the static sensitivity of the transducer, i.e. the midpoint deflection d_{max} or the voltage output/applied quasi-static pressure. For example, in figure 9 a speckle interferogram

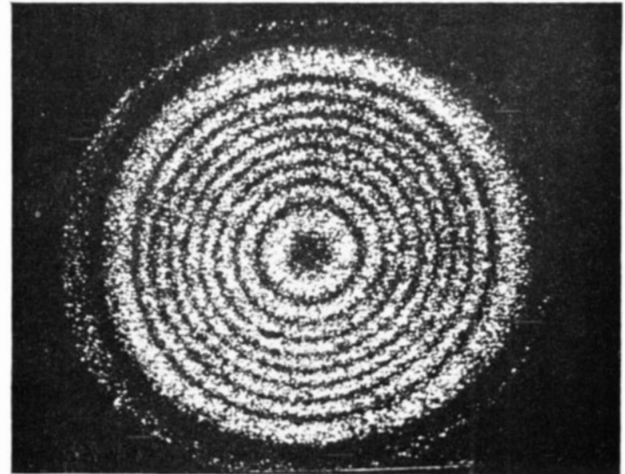


Figure 9 A real-time speckle interferogram of the diaphragm deflection of transducer A due to a static load of 1.67 kPa. The interferogram was photographed directly from the television monitor.

recorded in real time shows a deflection of $(2.7 \pm 0.1) \times 10^3$ nm in a 22.4 mm diameter, 0.22 mm thick diaphragm (transducer A). The applied pressure was 1.67 kPa.

4.2 Dynamic measurements

The oscilloscope traces shown in figure 10 represent a typical dynamic pressure measurement. The upper and lower traces correspond to the signal obtained with the fringe maxima and minima, respectively, centred on the detector aperture. Under these conditions the phase shift $\Delta\phi_{12}$ will produce a

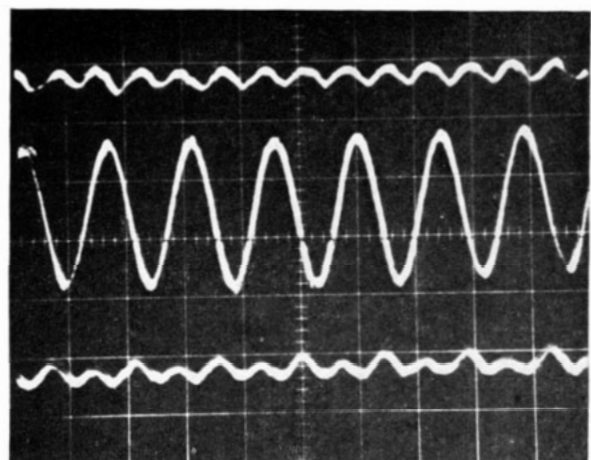


Figure 10 The measurement of sinusoidal pressure variation at a frequency of 3.20 kHz using the Michelson interferometer (vertical sensitivity 30 mV/division; sweep speed 2 ms/division).

minimum fluctuation in the intensity variation and this accounts for the small signal at doubled frequency which is observed. The voltage difference between the extreme level of these traces therefore corresponds to ΔV_c (260 ± 10 mV). The central trace was obtained with the aperture of the detector midway between fringe maxima and minima and therefore has peak-to-peak value ΔV_p . This result was obtained at a frequency of 3.26 kHz with the Michelson arrangement and corresponds to a peak pressure amplitude of 8.9 kPa. F_2 fringe field shifts (figures 3 and 4) were observed over the frequency range from 300 Hz to 1.1 kHz, and measurements were therefore not attempted in this region. A direct dynamic calibration result is shown in figure 11. Here the top trace is the output

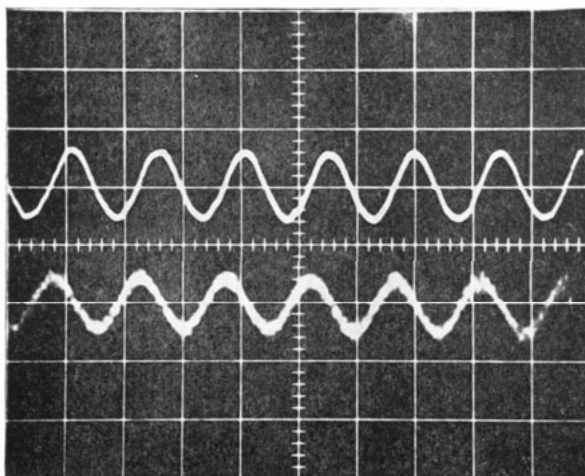


Figure 11 The direct comparison of transducer C output (lower trace, 1 mV/division) and interferometric pressure recording (upper trace, 50 mV/division). The frequency is 3.15 kHz.

from the Michelson interferometer which indicates a pressure variation of 0.13 kPa at a frequency of 3.15 kHz, and the bottom trace the corresponding voltage output (1 mV/division) from a strain gauge transducer. These traces were found to have practically identical Fourier spectra, indicating that the transducer had a very pure response at this frequency and pressure amplitude.

4.3 Some calibration results

The measurement techniques outlined above were used to obtain calibration results for four transducers:

A: a diaphragm transducer element 22.4 mm in diameter and 0.22 mm thick;

B: a transducer identical to A but of thickness 1.37 mm;

C and D: two nominally identical strain gauge transducers.

In all results the normalised sensitivity (sensitivity at frequency ν /sensitivity for quasi-static loading) is plotted against frequency and in figure 12 calibration results for near to quasi-static operation are shown. One would expect the transducers to have a normalised sensitivity of unity in this region and for B, C and D this was observed. Transducer A, however, exhibited a rapid and anomalous fall in response in passing from quasi-static to dynamic loading. This observation was repeatable and clearly indicates a significant experimental result. A quantitative interpretation is outside the scope of this paper but in this particular case the displacement of the fluid at the pressures under consideration (about 1 kPa) is of the same magnitude as the diaphragm deflection (approximately 10^3 nm, e.g. figure 9). Under these conditions the walls of the

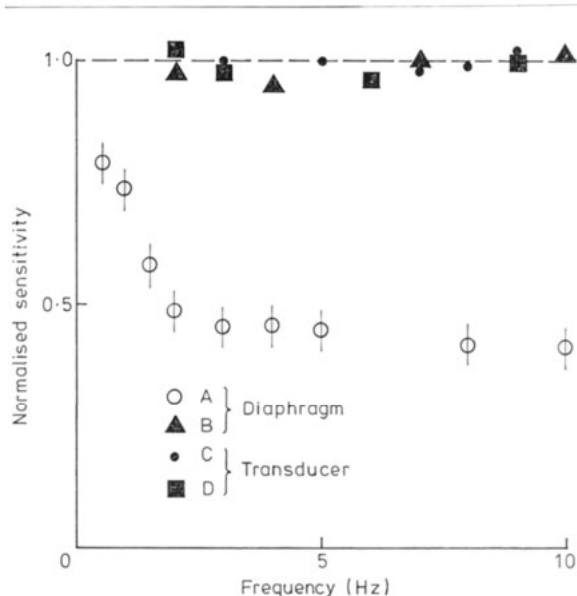


Figure 12 Low-frequency calibration results. Normalised sensitivity is plotted against frequency.

cavity can no longer be assumed to be rigid and one must consider the nature of the coupling between the diaphragm movement and the fluid displacement. The static sensitivities for the transducer are: A: $(1.36 \pm 0.03) \times 10^3$ nm kPa⁻¹; B: 62.5 nm kPa⁻¹; C: 12 ± 0.25 mV kPa⁻¹; and D: 10.25 ± 0.25 mV kPa⁻¹. Finally, the first resonance of transducer C is shown plotted in figure 13. (The pressure measurements have been corrected using $C(\nu)$.)

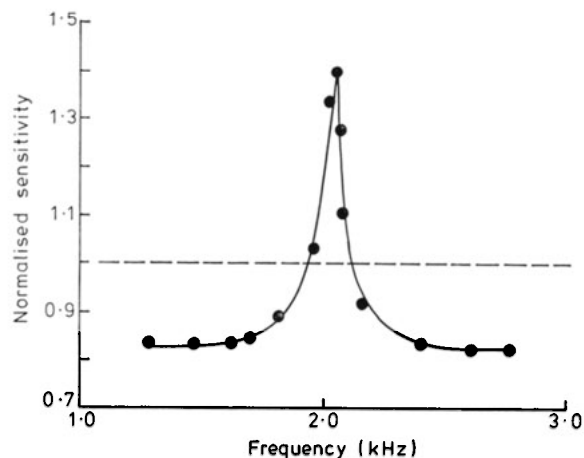


Figure 13 The first resonant peak of transducer C.

5 Discussion and conclusions

Interferometric techniques for the direct observation of quasi-static and dynamic pressure variations have been demonstrated. The major theoretical and practical problems have been solved and the existing apparatus has been used for routine transducer calibrations. Within the range of application no fundamental limitations exist, but to further extend the technique it will be necessary to:

- (i) isolate the cavity from the interferometric components in order to eliminate F_2 fringe field movements at all frequencies;
- (ii) shorten the cavity so that higher frequencies may be investigated within the region for which the simple $C(\nu)$ correction factor applies or preferably is very small; and

Interferometric pressure measurement

(iii) confine measurements to the Jamin arrangement so that the full pressure range is accommodated by a linear fringe shift.

For the existing method of excitation an additional problem arose at higher frequencies (above 1 kHz) where it was found that pressure variations sufficiently high to excite transducer B would not be transmitted into the oil. It may therefore be preferable to excite pressure variations in this frequency range by placing large piezoelectric crystals in direct contact with the oil. In considering (iii) it is interesting to note that the Jamin arrangement was particularly useful in the low-frequency (0–300 Hz) study of transducer B where the pressure variations sufficient to deflect the diaphragm caused phase shifts considerably greater than π in the Michelson arrangement. However, the smaller pressure variations readily detected at higher frequencies by the Michelson arrangement could not be detected above the noise in the Jamin output. A more complex fringe shift detector (e.g. a phase-sensitive detector) will therefore be necessary if (iii) is to be applied for all measurements. It would be interesting to investigate experimentally the form of $C(\nu)$, but unfortunately this would require a transducer of known linear response over the frequency range under consideration. However, condition (ii) can be satisfied for a wide frequency range (0–20 kHz) by halving the length of the existing cavity. Finally, the anomalous low-frequency result deserves more theoretical and experimental investigation. The latter could be carried out by measuring the response of diaphragms of identical diameter but gradually increasing thickness.

In some applications it may be unacceptable to use oil as the pressure-transmitting medium, but it should be noted that temperature variations will become significant if air is used and lead to erroneous interferometric measurements. (These temperature variations may also affect the transducer performance.) It has been noted elsewhere (*A Guide for the Dynamic Calibration of Pressure Transducers* 1972) that the presence of the fluid will affect the transfer function of the transducer, which will in turn change the resonant frequency and damping ratio. It would, however, be a relatively easy matter to quantify the former effects by directly measuring the free air resonance of the transducer diaphragms using electronic speckle pattern interferometry.

Acknowledgments

This work was supported by the Science Research Council. The authors would like to thank Professor J N Butters and also the technical staff of the Department of Mechanical Engineering for their support and encouragement.

References

- A Guide for the Dynamic Calibration of Pressure Transducers* 1972 (New York: American Society of Mechanical Engineers) ANSI B88.1
- Born M and Wolf E 1969 *Principles of Optics* (New York: Pergamon) pp 268–70
- Butters J N and Bergquist B D 1969 *Control* February 124–8
- Coulson C A 1955 *Waves* (Edinburgh and London: Oliver and Boyd) pp 60–5
- Jones R and Bergquist B D 1976 *The Engineering Uses of Coherent Optics*, ed E R Robertson (London: Cambridge University Press) pp 413–29
- Powell C P and Stetson K A 1965 *J. Opt. Soc. Am.* **15** 1593–8

Rayleigh J W S 1945 *The Theory of Sound* vol 1 (New York: Dover) pp 195–6

Rosen J S 1947 *J. Opt. Soc. Am.* **37** 932–5

Rosen J S 1949 *J. Chem. Phys.* **17** 1192–7

Thompson D H and Tanner L H 1969 *J. Phys. E: Sci. Instrum.* **2** 421–4